

Article

Not peer-reviewed version

---

# Futuristic Silicon Photonic Biosensor with Nanomaterial Enhancement for PSA Detection

---

[Timothy Okhai](#)<sup>\*</sup>, [Azeez Idris](#), [Usisjpho Feleni](#), [Lukas Snyman](#)

Posted Date: 8 January 2024

doi: 10.20944/preprints202401.0560.v1

Keywords: Biochemical sensors; Nanomaterials; Optical sensor; Prostate Specific Antigens; Receptor technology; Silicon Avalanche Mode LED; Silver nanoparticles



Preprints.org is a free multidiscipline platform providing preprint service that is dedicated to making early versions of research outputs permanently available and citable. Preprints posted at Preprints.org appear in Web of Science, Crossref, Google Scholar, Scilit, Europe PMC.

Copyright: This is an open access article distributed under the Creative Commons Attribution License which permits unrestricted use, distribution, and reproduction in any medium, provided the original work is properly cited.

Article

# Futuristic Silicon Photonic Biosensor with Nanomaterial Enhancement for PSA Detection

Timothy A. Okhai <sup>1,2,\*</sup>, Azeez O. Idris <sup>3</sup>, Usisipho Feleni <sup>4</sup> and Lukas W. Snyman <sup>2,4</sup>

<sup>1</sup> Department of Electrical Engineering, Faculty of Engineering and The Built Environment, Tshwane University of Technology, Pretoria, South Africa; okhaita@tut.ac.za

<sup>2</sup> Department of Electrical and Mining Engineering, College of Science, Engineering and Technology, University of South Africa, Florida, South Africa; snymalw@unisa.ac.za

<sup>3</sup> UNESCO-UNISA Africa Chair in Nanoscience and Nanotechnology, College of Graduate Studies, University of South Africa, Pretoria 392, South Africa; idrisalone4real@gmail.com

<sup>4</sup> Institute for Nanotechnology and Water Sustainability (iNanoWS), College of Science, Engineering and Technology, University of South Africa, Florida, South Africa; felenu@unisa.ac.za

\* Correspondence: okhaita@tut.ac.za; Tel.: +27 823 424 844

**Abstract:** This article describes a novel electrochemical on-chip biosensor that utilizes anti-PSA antibody (Ab) and silver nanoparticles (AgNPs) to enhance the sensing and detection capability of prostate specific antigen (PSA) in the blood. The AgNPs are prepared, characterized, and applied onto a silicon photonic on-chip biosensing receptor platform designed to enhance the accurate detection of PSA. The AgNPs were synthesized by a chemical reduction method using silver nitrate (AgNO<sub>3</sub>) as the precursor. Transmission electron microscopy (TEM), selected area electron diffraction (SAED), energy dispersion X-ray spectroscopy (EDS), small angle X-ray scattering (SAXS), X-ray diffraction (XRD) and light microscopy were among the methods used in the characterization and analysis of the AgNPs. Each stage of the immunosensor fabrication was characterized using cyclic voltammetry. The proposed immunosensor was applied in the detection of PSA, a prostate cancer biomarker, with a high sensitivity and a limit of detection of 0.17 ng/mL over a linear concentration range of 2.5 to 11.0 ng/mL. The immunosensor displayed good stability and was selective in the presence of interfering species like immunoglobulin (Ig) in human serum, ascorbic acid (AA) and diclofenac (Dic). The detectivity and sensitivity are significantly higher than previous reports on similar or related technologies.

**Keywords:** biochemical sensors; nanomaterials; Optical sensor; Prostate Specific Antigens; Receptor technology; Silicon Avalanche Mode LED; silver nanoparticles

## 1. Introduction

In recent years, research interest in nanomaterial technology, biosensors, biochemical sensors, and wearable diagnostic devices have experienced astronomical growth globally [1-4]. The vast research and market investment in these fields have also led to the development of better sensing techniques, new nanomaterials, and biomaterials like conducting polymers, copolymers, and sol-gels [5-7]. Additionally, the uses and application possibilities of these new-generation devices are now widely varied because they can be multiplexed and reduced to micro- and nano-dimensions and integrated on standard silicon integrated circuit chip [8-10]. Substantial advances have been achieved in producing these devices using technology emerging as light emitting devices that are functional in the silicon reverse-biased avalanche mode light emitting diode (Si AMLED) mode of operation [11-14]. An attractive route is to develop optically based sensors using technology where light emitting devices can be integrated with biosensing devices on chip for various purposes, such as detecting biomarkers, bacteria, toxins, and drugs [15-17]. The goal of this article is to present a novel means of PSA detection on a silicon photonic microchip incorporating optical waveguide and reflectometer technology on a nanomaterial-enhanced platform. This biosensor technology on a microsystem will

utilize a specific p+np+ graded junction type Si AMLED device that was realized in a 0.35  $\mu$  (micron) silicon bipolar process with a high-frequency RF application capability [18].

Prostate cancer is the most common cancer that poses a huge risk to men worldwide, and the lifetime risk for prostate cancer for South Africa men, according to the 2019 National Cancer Registry (NCR) is 1 in 15 [19]. To ensure survival and good treatment outcomes, it is extremely important to detect prostate cancer early. Thus, early detection for prostate cancer is achieved by quantifying the levels of prostate specific antigen (PSA), the biomarker for prostate cancer, in the blood [20]. The normal level of PSA in human serum is less than 4 ng/mL. A PSA level of more than 20 ng/mL is generally indicative of the presence of prostate cancer [21]. Generally, the standard method for the detection of PSA in most clinical settings is the widely known enzyme-linked immunosorbent assay (ELISA) [22]. However, this method is uneconomical for poorly resourced low-to-medium-income countries requiring expensive laboratory equipment, well-trained staff, and it takes roughly a day for results to be available. Therefore, a smart PSA detection technique that obviates these challenges by promising an effective, rapid and cost-effective detection method that is simple to use and accessible to low-resourced areas is highly desirable to reduce mortality and increase the rapid detection and survival rate of prostate cancer patients [23].

### *1.2. Development of IC Integrated SiLED Sensors*

The research conducted by Kramer et al. [24] and Snyman et al. [25] have resulted in several iterations of Light Emitting Devices (LEDs) in Standard Complementary Metal Oxide Silicon (CMOS) technology. The emission of light from these structures occurs through phonon-assisted intra-band and inter-band recombination phenomena [24-25]. The subsequent devices that were developed emitted more light when additional carriers were introduced into avalanching Si n+p light emitting junctions [25]. Xu et al. designed a series of complementary metal-oxide-semiconductor (CMOS) integrated LED devices with third terminal gated control [13].

Duttal and Steeneken et al. analyzed the carrier density, temperature, and electric field within the Si AMLEDs that operate in the forward-biased mode and emit in the 1100 nm region [26]. In a separate study, Xu and Snyman showed that Si AMLEDs in the 650-750 nm emission spectrum can improve the intensities of emission from 0.1 to about 200 nW/ $\mu\text{m}^2$ . They accomplished this by utilizing enhanced impurity scattering and extended E-field profiling in the device. A significant advantage of these devices is their ability to achieve high modulation speeds ranging into GHz due to the reverse bias configuration of Si AMLEDs [18].

Okhai et al. have reported the results of a detailed study conducted to analyse the dispersion characteristics of one of these devices per solid angle [27]. The radiation geometrical dispersion characteristics of a two-junction micro-dimension p $\pm$ np+ Silicon Avalanche Mode Light Emitting Device were analyzed for different wavelengths of light (colours) emitted at different emission angles from the surface of the device. The studies revealed that the dispersion characteristics of this device are dependent on the structure of the device, the topography of the various surface layers of the device, and the number of transparent over layers with each layer having a different refractive index [27] as shown in Figure 1. These studies have further opened novel application possibilities for this device in the design and development of futuristic on-chip electro-optical devices, which include micro- and nano-dimensioned biosensors.

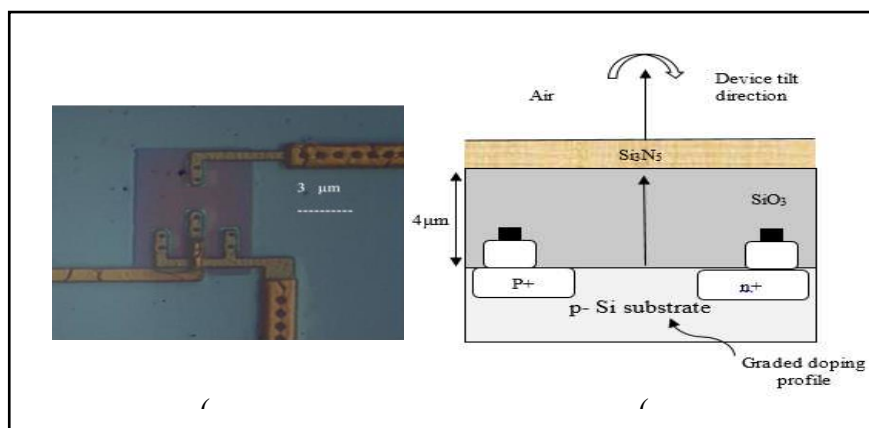


**Figure 1.** (a) Bright field electron micrograph of the Si Avalanche Mode LED [13], and (b) device schematic revealing the device's over layers.

Optical biosensors that use evanescent wave for biomolecular interaction can be used for direct and rapid measurements in real-time, especially when integrated with optical components like light emitters, optical detectors, optical waveguides, and other related optical technology on a single substrate. These devices have the added advantage of allowing the flexible design of compact sensors and combining many sensors on a single chip. Additional benefits of integration include miniaturization, robustness, reliability, low energy consumption, low production costs due to mass production, and ease of aligning individual optical elements [28].

### 1.3. Waveguide, evanescent field, and receptor layer

An optical waveguide has a core and cladding with different refractive indices which permit light to be guided through the core due to total internal reflection, resulting in the creation of an evanescent optical field that diminishes exponentially from the sensor surface. This is illustrated in Figure 2. The refractive index contrast is modulated by biomolecular binding events, which attenuate light propagation through the waveguide. Optical biosensors can be constructed that detect specific molecules using light waves to measure how they move through a specially designed waveguide, as shown in Figure 2.

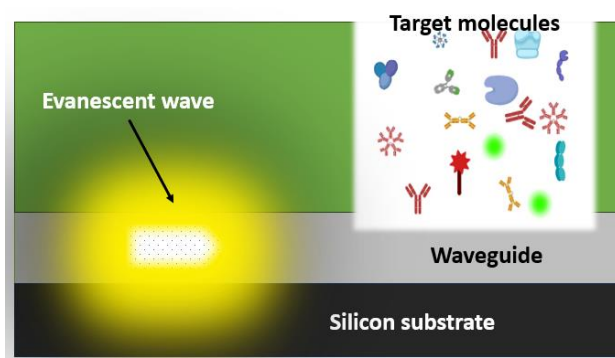


**Figure 2.** Evanescent wave, waveguide and receptor layer in an optical biosensor design.

The immobilization of capturing probes on the surface to form the capturing spot is a challenge for integrated biosensors, regardless of the transduction technique used. In order to improve the target analyte's selective absorption, our design uses AgNPs as an immobilization layer in the receptor cavity, which is created by etching a receptor cavity through the silicon substrate.

Microdisplays and Lab-on-a-chip systems are among the applications for Si Av LEDs that have already been suggested and proven [28–32]. Evaluations of the device's test results provide fresh insights into how the derived technology might be used in cutting-edge integrated on-chip optoelectronic and biosensor applications. Of particular importance is the recent success in increasing

the emission intensity to about 100-fold, reduction of the device's size to micron emissions, and the emission areas to submicron dimensions [33]. The different methods used to accomplish these applications through micro- and nano-lithographic techniques, and to create micro-electronics processing devices have been discussed in another study [34]. The prepared AgNPs is use in the biointeraction area that has been etched in the nitrite layer to form a region that allows for the selective detection of PSA and other biomarker, depending on the material used to construct the sensing platform. While the AgNPs detection platform's application for the enhancement of PSA detection is just one possibility, other possible applications have been demonstrated in recent studies. The use of AgNPs as an effective anticancer agent as deployed in a biosensor platform have been demonstrated by several studies to date. Hepukur et al. have evaluated the use of silver AgNPs/capecitabine to treat breast cancer cells [35]. In their study, they showed how the number of early and late apoptotic cells were considerably increased on MCF-7 cells by drug-bonded AgNPs. In another study, Majeed et al. used AgNPs capped with bovine serum albumin (BSA). They observed that the anticancer effect of capped AgNPs (cAgNPs) showed the IC50 value against breast cancer MCF-7 at 80  $\mu\text{g/mL}$ , intestinal colon cancer HCT- 116 at 60  $\mu\text{g/mL}$ , and bone cancer osteosarcoma MG-63 cell at 80  $\mu\text{g/mL}$  while against normal fibroblast cells 3T3 cells showed the IC50 value at 140  $\mu\text{g/mL}$  [36].

## 2. Materials and methods

In this study, AgNPs were synthesized, characterized, and used to prepare an immunosensor platform to increase the signal response, thereby creating an intelligent biosensor for the detection of PSA. The following sections provide further detail about the synthesis techniques, materials utilized, characterization procedure, and the results.

### 2.1. Synthesis of silver nanoparticles: materials and methods

The AgNPs were synthesized by a protocol adapted from Muzamil et al., with a slight modification [37]. The chemicals used were Trisodium citrate ( $\text{Na}_3\text{C}_6\text{H}_5\text{O}_7$ , 1%), Silver nitrate ( $\text{AgNO}_3$ ,  $\geq 99\%$ ), Sodium hydroxide ( $\text{NaOH}$ ,  $\geq 99\%$ ) and Polyethylene glycol ( $\text{C}_{2n}\text{H}_{4n+2}\text{O}_{n+1}$ ,  $\geq 99\%$ ). All of these analytical grade chemicals were purchased from Sigma Aldrich. A chemical reduction method was used in the synthesis of AgNPs, with silver nitrate ( $\text{AgNO}_3$ ) acting as the silver precursor. The experiment was performed under room temperature conditions (23  $^\circ\text{C}$ ). The synthesis of AgNPs was realised by combining 50 mL of a 1 mM silver nitrate solution with 5 mL of polyethylene glycol and heated to boiling point on a magnetic stirrer. When the solution started to boil, 4 mL of a 1% trisodium citrate solution was rapidly introduced while stirring constantly. In about 2 – 3 mins afterwards, the solution transformed into a yellow colour, confirming the formation of AgNPs. The nanoparticles' pH was maintained at 7.6 through the addition of 0.5 M NaOH. Afterwards, the solution was cooled down to room temperature and stored at 4  $^\circ\text{C}$  for later use.

### 2.2. Characterization of the silver nanoparticles

In the characterization of the AgNPs, different analytical instruments and techniques were used. The JSM-7800F Field Emission Electron Scanning Microscope (FESEM) was used to examine the surface structure and elemental signature of the silver nanoparticles, paired with energy-dispersive x-ray spectroscopy (EDS). The study of the nanomaterials' functional groups was carried out on a Frontier Perkin Elmer fourier reansform infra-red (FTIR) spectrometer (Spectrum 100 spectrometer) within a wavelength range of 400-4000  $\text{cm}^{-1}$ , utilizing the KBr pellet technique. GIFT software was used to Fourier-transform the scattering data to achieve the pair distance distribution function (PDDF) and size distribution spectra. Ultraviolet visible (UV-Vis) spectral data, spanning from 200 to 800 nm, were obtained using a Lambda 650S UV/Visible Spectrometer by Perkin Elma. High-resolution transmission electron microscope (HRTEM) analysis was completed via a Hitachi H-800 electron microscope, operating at a 200kV acceleration, to establish the elemental composition and size distribution of the samples. The scanning electron microscope (SEM) images of the samples were

taken using a JSM-6400 JEOL Scanning Microscope. Small-angle x-ray scattering (SAXS) spectroscopy was accomplished using an Anton-Paar SAXSpace Spectrometer, sourced from Graz, Austria. SAXdrive software was employed to generate X-ray scattering spectra. All the data obtained from the characterization equipment were plotted using Origin 8.0 Software. The SEM, FESEM, HRTEM, fourier transform infra-red (FTIR) Spectroscopy, and ultraviolet-visible (UV-Vis) spectroscopy results have been published in our previous work [34]. In this present article, we present only the SAXS, X-ray diffraction (XRD) and light microscope analysis of the AgNPs.

### 2.3. Experimental results and discussion

The TEM image depicted below illustrates that AgNPs are spherical in shape at a nano-scale level, with an internal crystalline structure. This is confirmed by the accompanying Selected Area Electron Diffraction (SAED) image in the insert. Moreover, insights from the HRTEM complement the SAXS findings, confirming that the majority of particles are either spherical or cube-shaped.

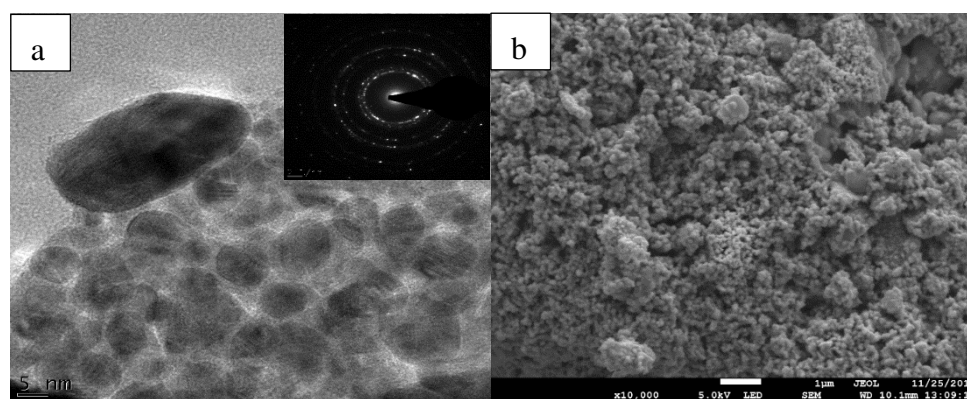


**Figure 3.** (a) TEM image and the SAED pattern insert for the AgNPs (b) SEM photomicrograph image at x10,000 magnification.

The SAXS analysis displayed in Figure 4 was used to probe the internal composition of the nanoparticles. It demonstrated that the AgNPs exhibit lattice fringes, solidifying the idea that the particles have a crystalline nature. Furthermore, they presented a quasi-spherical shaped internal configuration as anticipated. Within the internal composition, Figure 4 (a) exhibits the intensity-based size dispersion, while 4 (b) illustrates the volume-based size dispersion.

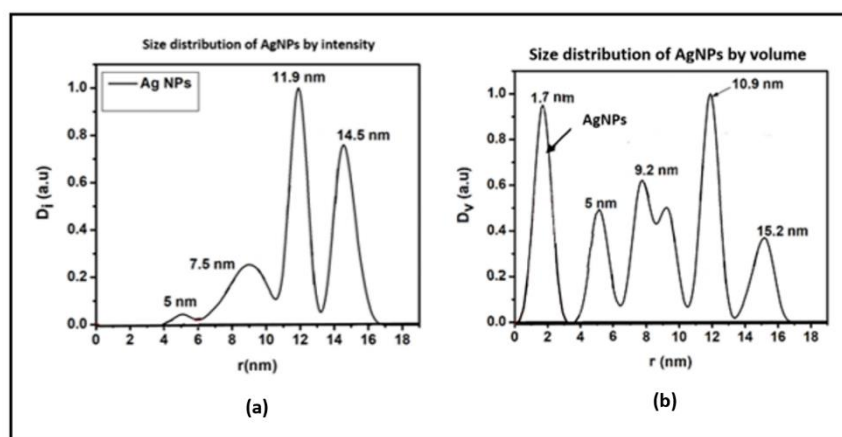


**Figure 4.** SAX space analysis of AgNPs showing (a) the size distribution by intensity and (b) the size distribution by volume.

Energy dispersion X-ray spectroscopy (EDS) was used to determine the elemental composition of the AgNPs, as illustrated in Figure 5. The presence of oxygen, carbon, and silver is confirmed by the EDS spectrum analysis. The strong indication of carbon was a result of the carbon tape that was

used for collecting and adhering the nano particles during sample preparation for the EDS analyses. The small presence of sodium seen is possibly due to miniscule impurities in the carbon.

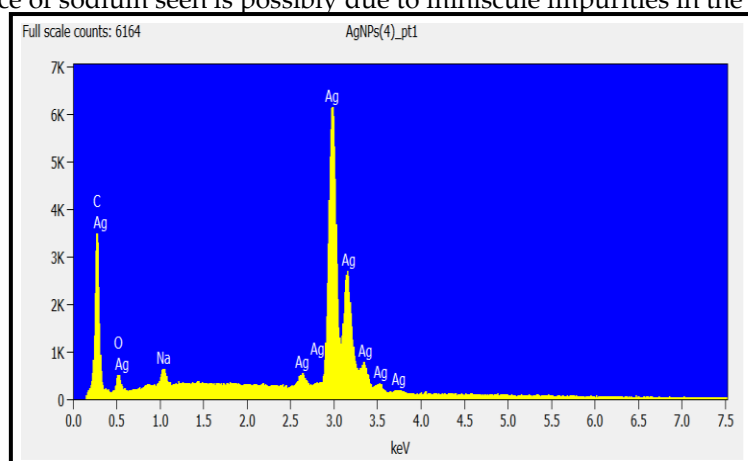


**Figure 5.** EDS spectrum proving that silver, carbon, and oxygen are present.

The EDS analysis reveals that Ag is the predominant element present in the produced nanoparticles. The observed morphology and elemental analyses are consistent with expected results for silver nanoparticles that were functionalized/synthesized with polyethylene glycol. Quite a high spread in particle size was observed ranging from 1.7 nm to 15 nm. The highest average size seems to be about 15 nm with variation in size on both sides as confirmed by the SAX analysis in Figure 4 (a). The presence of a large number of topographically small particles of 2- 8 nm (Figure 4 (b)) is particularly relevant and important for our study. The average-sized particle substantially increases the surface area of the layers produced and is ideal for adhering reactant pathogen species to the nanoparticles. Some particles at nm scale may penetrate bacterial cell walls during aqua-based interaction processes and disrupt the enzyme-based reproduction processes inside the cells.

To confirm the crystal structure of the synthesized AgNPs, X-ray diffraction studies were carried out using PANanalytical XRD machine, and High Score software for analysis. The scanned XRD pattern is shown in Figure 6. The diffracted intensities were recorded from  $20^\circ$  to  $90^\circ$  at 2 theta ( $2\Theta$ ) angles. The diffraction peaks match the characteristic crystalline Face Centred Cubic (FCC) silver lines, which are consistent with the standard powder diffraction card of Joint Committee on Powder Diffraction Standards (JCPDS), silver file No. 04-0783 [37]. The powdered AgNPs show a cubic structure with characteristic diffraction peaks at scattered angles  $2\Theta = 38.598, 45.183, 64.291, 77.172$  and  $81.339$  which are assigned to (111), (200), (220), (311) and (222) planes respectively [38 – 41]. The peak corresponding to (111) is more intense than the other planes suggesting that (111) is the predominant orientation and the synthesized AgNPs are crystalline in nature. These results agree perfectly with similar results that have been reported earlier for AgNPs [37-41]. These peaks indicate that the AgNPs were well-crystallized. Furthermore, the planes revealed that the AgNPs are face centred cubic structured (JCPDS 89-3722) [42].

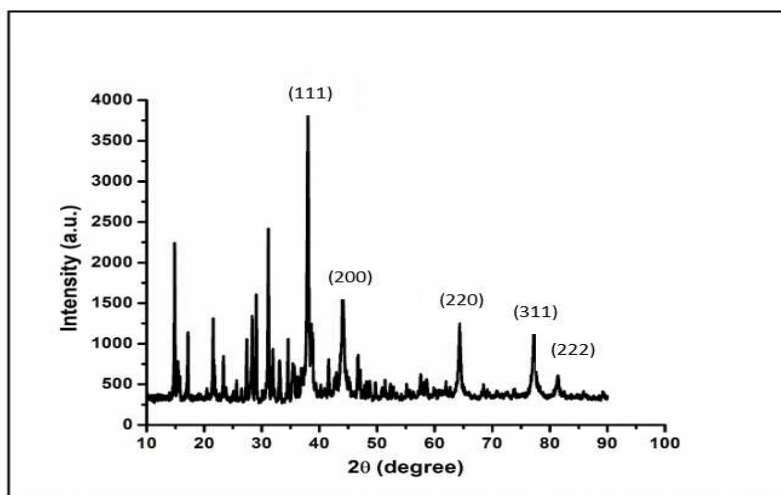


**Figure 6.** X-ray diffraction pattern of the synthesized AgNPs.

To determine the reflective property of the AgNPs, several photomicrograph images of the silver nanoparticles were obtained at different magnifications.

The Leica DMI8A Inverted microscope was used. AgNPs were placed in a glass slide and positioned on to the microscope for observation at different magnifications from  $\times 20$  to  $\times 100$ . The Leica Application Suites (LAS) Software was used to process the images obtained. The images obtained in Figure 7 show high optical reflection with increasing magnification from (a) to (f).

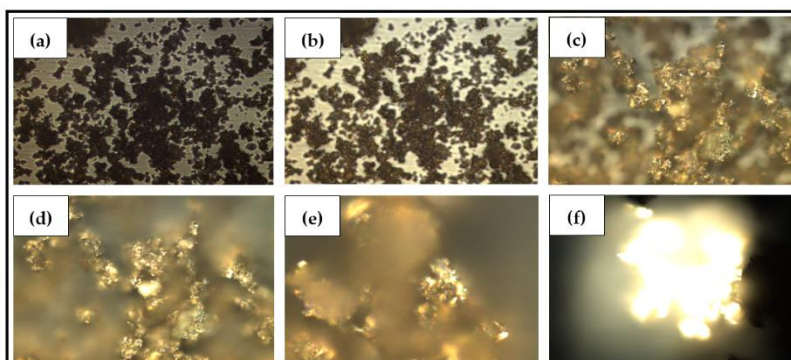


**Figure 7.** Photomicrographs from the Leica DMI8 Inverted microscope.

### 3. Development of PSA biosensor using AgNPs

To demonstrate the application of AgNPs as an effective sensing platform for prostate cancer detection, an immunosensor was prepared and characterized using electrochemistry experimental methods to determine its key sensing parameters like stability, interference, selectivity, and sensitivity. The monoclonal anti-PSA antibody (Ab) produced from human serum, PSA from human semen, and bovine serum albumin (BSA) that were used in this application were all purchased from Sigma Aldrich. To prepare the immunosensor, first 0.1M PBS (Phosphate buffer solution) of pH 7.4 was prepared. Then, 5 ml of this PBS was measured into a glass vial and cyclic voltammetric (CV) studies were run on a bare glassy carbon electrode (GCE) at scan rate of 30 mV/s in the potential window -2 to +2 V. After obtaining the CV plot, the bare GCE was modified with AgNPs and left to dry overnight at room temperature. Then, CV of the GCE/AgNPs was run at scan rate of 30 mV/s in the potential window -2 to +2 V. Same was done after modification with GCE/AgNPs and Ab. The GCE//AgNPs/Ab was modified with BSA to form the immunosensor GCE/AgNPs/Ab/BSA. A further CV of this immunosensor was obtained and plotted. Lastly, 0.5  $\mu$ G of PSA was prepared and dropped into the 0.1 M PBS at pH 7.4, following which the CV of the immunosensor (GCE/AGNPs/Ab/BSA) was run at scan rate of 30 mV/s in the potential window -2 to +2 V. A plot of the

GCE/AgNPs/Ab/BSA/PSA was then obtained. A schematic representation of the electrochemical immunosensor fabrication process is shown in Figure 8.

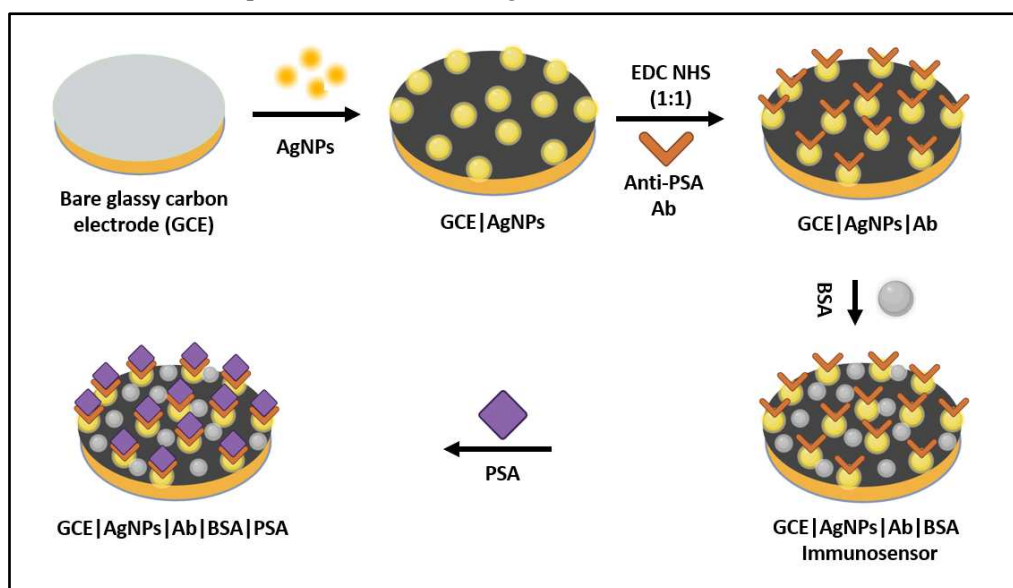


**Figure 8.** Electrochemical immunosensor fabrication flow process.

Figure 9 shows the CV measurements that compare the characteristic features of (a) bare GCE, (b) GCE|AgNPs, (c) GCE|AgNPs|Ab, (d) GCE|AgNPs|Ab|BSA, and (e) GCE|AgNPs|Ab|BSA|PSA in 0.1 M PBS of pH 7.4 at scan rate of 30 mV/s at the potential window -2 to 2 V. As seen in the plot, the bare GCE showed no response. But when modified, the presence of the AgNPs on the bare GCE modified electrode (curve b) resulted in a significant increase in the current response. One prominent oxidation peak at 0.25 V as well as two reduction peaks at -0.74 V and -0.27 V are observed for (c) GCE|AgNPs|Ab (curve c). The peaks are assigned to the interactions between carboxylic and amino groups from polyethylene glycol (PEG) capped AgNPs and antibody [43]. Such an enhancement is associated with an enhanced electron transfer from the electrode to buffer solution.

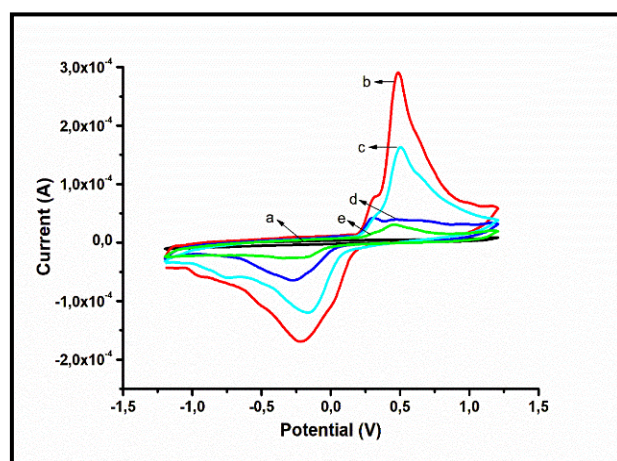


**Figure 9.** CV measurements of immunosensor platform for (a) Bare GCE (b) GCE|AgNPs, (c) GCE|AgNPs|Ab, (d) GCE|AgNPs|Ab|BSA, and (e) GCE|AgNPs|Ab|BSA|PSA in 0.1 M PBS of pH 7.4 at scan rate of 30 mV/s in the potential window -2 to 2 V.

Electroactive charged bare glassy carbon electrode surfaces can be used to immobilize antibodies in a way that is sensitive and specific. This makes them a good choice for developing electrochemical biosensors [44]. Therefore, the GCE|AgNPs surface serves as a good environment for antibody immobilization. This leads to improved PSA sensing limitations [45]. Additionally, there is a decrease

in the electrochemical current response for the GCE|AgNPs|Ab|BSA (curve (d)). Furthermore, a resistance in charge transfer is expected at this point because of the insulating property of BSA. This also confirms that the BSA is effectively immobilized on the surface of the electrode thereby blocking most non-binding sites. The blockage leads to a reduction in the available electroactive surface that is accessible, which further results in a reduction in the magnitude of the current [46]. In curve (e), the current decreased due to hindrance in electron transfer caused by the capture of PSA by its antibody in GCE|AgNPs|Ab|BSA|PSA for 10 ng/mL PSA. It is noteworthy that the capture led to a slight shift of the reduction peak due to the immunosensor surface modification [47].

### 3.1. Stability studies of AgNPs immunosensor

The storage stability of the GCE|AgNPs|Ab|BSA sensor was examined by CV in 0.1 M PBS (pH 7.4) containing 5  $\mu$ G of PSA. Two storage conditions were investigated: darkroom storage at room temperature, and refrigerated storage at 4 °C. In the first experiment, the sensor was stored at room temperature in a darkroom for 5 days. After this period of storage, the result indicates a 55% decrease in the peak current of the sensor compared to the initial response (Figure 10 (a)). In the next experiment, the sensor was stored in a refrigerator at 4 °C. After 5 days of storage under this condition, the result indicates that the sensor retained 93% of its initial response (Figure 10 (b)). With these results, it is clear that the sensor retains its integrity much better when stored in a refrigerated condition at 4 °C. Therefore, the results show that the sensor was stable for PSA detection over a 5-day storage period.

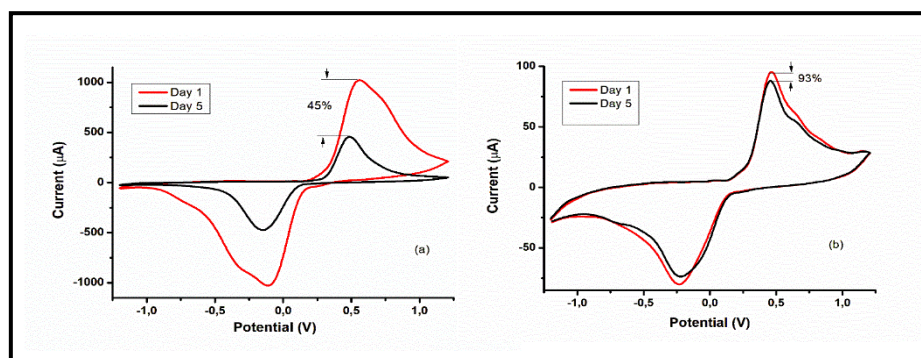


**Figure 10.** Stability Studies: CV of immunosensor in 0.1 M PBS of pH 7.4 at scan rate 30 mV/s in the potential window of -2 to 2 V after adding 5  $\mu$ G PSA at day 1 and after day 5, showing a retention of 45% in dark room storage (a), and 93% in refrigerated storage (b).

### 3.2. Sensitivity studies

To determine the sensitivity, the prepared immunosensor was used to detect different concentrations of PSA ranges from 2.5 to 11.0 ng/mL.

The exponential plot in Figure 11 (a) shows that the analyte of interest has reached a saturation point. Figure 11 (b) is the linear regression plot with the linear region having less points fitted in line as derived from the exponential plot.

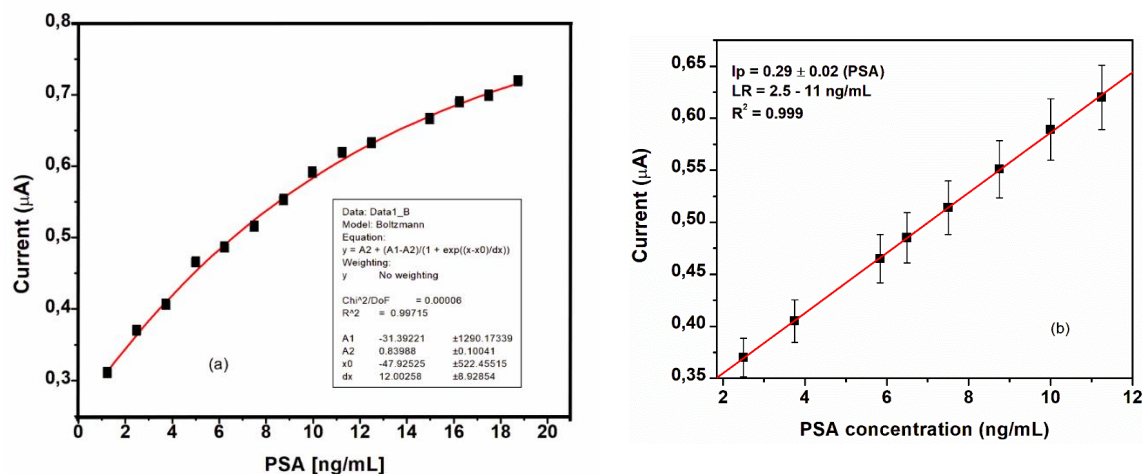


**Figure 11.** Exponential plot (a) and linear regression plot (b) of current versus concentration derived from the exponential plot for the PSA immunosensor.

As expected, the response signal decreased with the increase of PSA concentration. The current change was proportional to PSA concentration in the range from 2.5 to 11.0 ng/mL with a sensitivity of  $0.29 (\pm 0.20)$  A/(ng/mL), and the limit of detection was calculated as 0.17 ng/mL. The  $R^2$  value is given as 99.99%. The normal level of PSA in human serum is less than 4 ng/mL. A PSA concentration value over 20 ng/mL in human serum is indicative of the presence of prostate cancer [48]. Table 1 shows the proposed method with already reported PSA immunosensors.

**Table 1.** Comparison of the proposed method with already reported PSA immunosensors.

Immunosensor/Electrode material	Detection method	Linear range (ng/mL)	LOD (ng/mL)	References
AuNPs/CHI/SPE	CV, SWV	1 - 18	$1.0 \times 10^{-3}$	49
GS-QD-Ab2	SWV	$5.0 \times 10^{-3}$ - 10	$3.0 \times 10^{-3}$	50
GS-MB-CS	CV	$5.0 \times 10^{-2}$ - 5	$1.3 \times 10^{-2}$	51
BSA/Ab/TGA/OsTezQD/PPy	CV	0 - 15	$3.6 \times 10^{-1}$	52
Anti-KLK3/APBA/6-PICA	SWV	$5.0 \times 10^{-1}$ - 100	$1.1 \times 10^{-1}$	53
GC/rGO-Chit/Ab/PSA/AuNPs-PAMA-Aptamer	EIS	$5.0 \times 10^{-3}$ - 35	$5.0 \times 10^{-3}$	54
HQ@CuNPs-reduced-fullerene-C60/GCE	CV, EIS	$5.0 \times 10^{-3}$ - 20	$2.0 \times 10^{-3}$	55
HDT.SAM/AuNPs/anti-PSA	SWV	$2.0 \times 10^{-1}$ - 200	$1.0 \times 10^{-2}$	56
AuNPs-Gr/GCE	Amperometry	0 - 10	$5.9 \times 10^{-1}$	57
MWCNTs	EIS	0 to 500	1.18	58
GCE/AgNPs/Ab/BSA	CV	2.5 - 11	$1.7 \times 10^{-1}$	This work

The LOD values reported by Gupta et al. [52], Oliveira et al. [57], and Jang et al. [58] are  $3.6 \times 10^{-1}$ ,  $5.9 \times 10^{-1}$  ng/mL and 1.18 ng/mL, respectively. These reported values are respectively 2.1, 3.5 and 6.9 orders of magnitude higher than the LOD obtained in this current work. These results show that the proposed immunosensor in this study is very sensitive for PSA detection. The detection range

and sensitivity of the prepared sensor are within the range to diagnose the early stage of prostate cancer ( $> 4$  ng/mL of PSA). The sensor can be manufactured in micro dimensions on a microchip, making it of extremely small size and very cost effective. The optical and noise-free architecture, sensitivity and rapid detection ability (results can be available within an hour), are additional advantages of the proposed immunosensor. The detection limit of  $1.7 \times 10^{-1}$  is also about 10 times higher than ELISA, which has a PSA detection limit of less than 1 ng/mL [59-60]. These attractive properties make the proposed immunosensor more advantageous than ELISA for deployment in poorly resourced rural settings for the rapid detection of PSA.

### 3.3. Interference studies

The interfering species employed include immunoglobulin (Ig) in human serum, Ascorbic acid (AA) and Diclofenac (Dic), a commonly used anti-inflammatory drug. In terms of methodology, two options for determining the effects of interfering species on the sensor|PSA were adopted. The first method was to study the effect of addition of the interferents separately on the Sensor|PSA and record the CV for each interferent. The second option, which was the method used in this study, was to do a CV run for Sensor|PSA, with successive addition of equal volumes of the interfering species, i.e., Sensor|PSA|Ig, Sensor|PSA|Ig|AA and Sensor|PSA|Ig|AA|Dic.

Figure 12 shows the interference bar graph. To evaluate the selectivity of the sensor (GCE|AgNps|Ab|BSA|PSA), the effect of some potential interferents on the determination of 10 nM PSA was investigated. As shown in Figure 12, the electrochemical response of the immunosensor with each addition showed a slight progressive downward change in the peak current in the potential window -2 V to +2 V in the presence of the interfering species. It was found that these compounds impact slightly on PSA detection when all three interfering drugs are present in equal volumes as the PSA. Thus, the results indicate that the stability of the proposed sensor is slightly decreased when all three interfering species are present in equal volumes as the PSA.

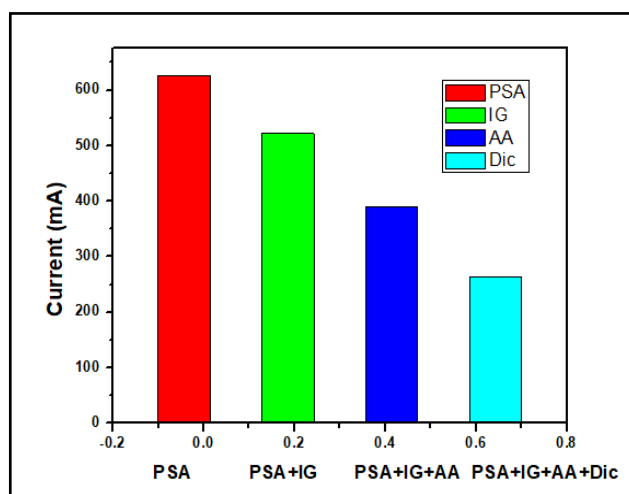


**Figure 12. Interference studies,** CV of immunosensor in 0.1M PBS of pH 7.4 at scan rate 30 mV/S in the potential window -2 to 2 V (a) after adding PSA to immunosensor (Sensor|PSA (b) Sensor|PSA|Ig (c) Sensor|PSA|IG|AA (d) Sensor|PSA|IG|AA|Dic.

## 4. Application in the design of microelectronic optical and chip-based biosensors

This section outlines the design of the device and its potential use as a PSA immunosensor platform incorporated on-chip.

### 4.1. Application in new micro- and nano-dimensioned devices

RSoft BeamProp optical simulation software was used to simulate the interaction between evanescent waves and biological samples within a biointeraction region etched into the nitrite layer

illuminated by light waves moving through the waveguide. Radiated light is steered through the waveguide resulting in an evanescent wave which depreciates on an exponential scale as the distance from its origin increases. Figure 13 illustrates the optical biosensor design with the evanescent wave, waveguide and receptor region enhanced with nanomaterials. It also illustrates how this wave travels through the waveguide to the etched biointeraction region to interact with a particular analyte material attached to nanomaterials inside the cavity. Microdisplays and novel biosensor devices are among the applications for Si Av LEDs that have been suggested [29–31].

Examining the test outcomes from our tool reveals promising prospects for the practical use of the developed technology in forward-thinking integrative on-chip optoelectronic and biosensor design for PSA identification. As shown in Figure 13, the synthesized AgNPs is deployed in the biointeraction region within the device to form a highly sensitive biosensor platform for selective detection of analytes like PSA. While the application of AgNPs detection platform for enhancement of PSA detection is just one possibility, other possible applications have been demonstrated in recent studies.

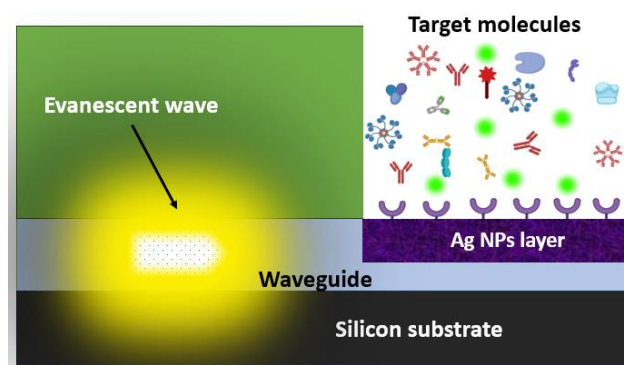


**Figure 13.** Optical biosensor design with evanescent wave, waveguide, and receptor layer enhanced with nanomaterials.

The use of AgNPs as an effective anticancer agent as integrated in a biosensor platform in this study is comparable to several studies which have demonstrated the efficacy of AgNPs and its composites for cancer therapy [35-36].

## 5. Conclusions

In this work, an immunosensor based on GCE|AgNPs|Ab|BSA as sensing platform has been successfully prepared for integration in a recessed cavity on a silicon photonic chip for the detection of PSA, a prostate cancer biomarker. The prepared immunosensor showed satisfactory stability, reproducibility, and selectivity. The detection range of 2.5 – 11 ng/mL, and a detection limit of  $1.7 \times 10^{-1}$  ng/mL were achieved, making it attractive for the diagnosis of the early stages of prostate cancer ( $> 4$  ng/mL of PSA). When choosing a design for detecting PSA, the difference in sensitivity is not the only thing to consider. Conventional tests have problems with accuracy and consistency, which can lead to incorrect results [23]. To be useful in a clinical setting, a sensor must produce reliable and consistent results. This is why nanotechnology, combined with an optical, noise-free, silicon photonic architecture is being researched for this application, as it has the potential to produce more accurate and reliable results. This proposed design also solves some of the problems faced by currently available ELISA test used in clinical settings. The PSA detection test is simple, non-invasive, easy to use and does not require skilled personnel or expensive laboratory equipment or space. It has the advantage of rapid deployment in remote rural settings or in the doctor's office. In addition, once validated and optimized, this sensor can be easily fabricated and produced inexpensively at commercial scale as a lab-on-a-chip device due to the micro- and nano dimensions of the microchip.

What we have demonstrated in this study is proof of concept. Future perspective will include (1) extending this work to utilize real human samples from body fluids for PSA detection, (2) broaden the application to include the detection of other cancer biomarkers such as carcinoembryonic albumin

(CEA), a biomarker for colorectal cancer, epidermal growth factor receptor (EGFR), a biomarker for lung cancer, and alpha fetoprotein (AFP) a biomarker for liver cancer, and (3) detect a host of other biomolecules by using other bio-specific materials. In our design, we have proposed further application in developing a new generation of biosensors integrated on a silicon photonic microchip. These sensors can detect a variety of analytes by combining a receptor cavity interaction layer, evanescent waves propagated through a waveguide, and an array of detectors. Optical signal change unique to the absorbed species is detectable from either the difference in refractive indices or through the coupling of evanescent radiation fields with sample analytes in the recessed cavity. The sensitivity and selectivity of these biosensor devices can be greatly enhanced by creating a layer of nanomaterials in the receptor cavity, as demonstrated in this work.

**Author Contributions:** “Conceptualization, Okhai, T.A. and Snyman L.W.; methodology, Okhai, T.A.; Snyman L.W.; Idris, A.O, and Feleni U.; software, Okhai, T.A. and Snyman, L.W.; validation, Snyman, L.W. and Feleni U; formal analysis, Okhai, T.A, and Idris, A.O.; investigation, Okhai, T.A. and Idris, A.O.; resources, Okhai, T.A.; data curation, Okhai, T.A.; writing—original draft preparation, Okhai, T.A.; writing—review and editing, Snyman, L.W. and Feleni, U. Visualization, Okhai, T.A.; supervision, Snyman, L.W., and Feleni, U.; project administration, Okhai, T.A.; funding acquisition, Okhai, T.A., and Snyman, L.W. All authors have read and agreed to the published version of the manuscript.”

**Funding:** This research was supported in part by the National Research Foundation of South Africa, Key International Collaboration Grant (KIC 69798), and the Department of Higher Education and Training (DHET) Grant administered by the Tshwane University of Technology, South Africa. Partial support was also received from the Institute of Nanotechnology and Water Sustainability, University of South Africa.

**Institutional Review Board Statement:** The study was conducted in accordance with the Declaration of Helsinki, and approved by the SOE Ethics Review Committee of THE UNIVERSITY OF SOUTH AFRICA (protocol code 2019/CSET\_SOC/TAO/001 and date of approval 26/09/2019).” For this study.

**Informed Consent Statement:** Not applicable.

**Data Availability Statement:** No new data were created or analyzed in this study. Data sharing is not applicable to this article.

**Acknowledgments:** Special acknowledgement and thanks to the iNanoWS Laboratory at UNISA, South Africa, for supporting the experimental work and facilitating the nanomaterials analysis and characterization. The RF and Opto-Electronics Laboratory at ESIEE-Paris, France is also acknowledged for the initial device design and experimental work.

**Conflicts of Interest:** The authors declare no conflict of interest. The funders had no role in the design of the study; in the collection, analyses, or interpretation of data; in the writing of the manuscript, or in the decision to publish the results.

## References

1. Chauhan, N.; Saxena, K.; Tikadar, M.; Jain, U., Recent Advances in the Design of Biosensors Based on Novel Nanomaterials: An Insight. *Nanotechnol. Precis. Eng.* 2021, 4, 045003; DOI: <https://doi.org/10.1063/1.50006524>.
2. Zolti, O.; Suganthan, B.; Ramasamy, R.P. Lab-on-a-Chip Electrochemical Biosensors for Foodborne Pathogen Detection: A Review of Common Standards and Recent Progress. *Biosensors* 2023, 13, 215; <https://doi.org/10.3390/bios13020215>.
3. Vorobjova, A.; Tishkevich, D.; Shimanovich, D.; Zdorovets, M.; Kozlovskiy, A.; Zubar, T.; Vinnik, D.; Dong, M.; Trukhanov, S.; Trukhanov, A.; et al. Electrochemical Behaviour of Ti/Al<sub>2</sub>O<sub>3</sub>/Ni Nanocomposite Material in Artificial Physiological Solution: Prospects for Biomedical Application. *Nanomaterials* 2020, 10, 173. <https://doi.org/10.3390/nano10010173>.
4. Mehmood, S.; Ali, Z.; Khan, S.R.; Aman, S.; Elnaggar, A.Y.; Ibrahim, M.M.; Zubar, T.I.; Tishkevich, D.I.; Trukhanov, S.V.; Trukhanov, A.V. Mechanically Stable Magnetic Metallic Materials for Biomedical Applications. *Materials* 2022, 15, 8009. <https://doi.org/10.3390/ma15228009>.
5. Namsheer, K.; Rout, C.S. Conducting Polymers: A Comprehensive Review on Recent Advances in Synthesis, Properties and Applications. *RSC Adv.* 2021, 11, 5659–5697; DOI: <https://doi.org/10.1039/d0ra07800j>.
6. Singh, N.; Riaz, U., Recent Trends on Synthetic Approaches and Application Studies of Conducting Polymers and Copolymers: A Review. *Polym. Bull.* 2022, 79, 10377–10408; DOI: <https://doi.org/10.1007/s00289-021-03987-1>.

7. Yang, S.; Liu, Z.; Pan, Y.; Guan, J.; Yang, P.; Asel, M. A Review of Research Progress on the Performance of Intelligent Polymer Gel. *Molecules* 2023, 28, 4246; <https://doi.org/10.3390/molecules28104246>.
8. Mariani, F.; Gualandi, I.; Schuhmann, W.; et al. Micro- and Nano-Devices for Electrochemical Sensing. *Microchim. Acta* 2022, 189, 459; DOI: <https://doi.org/10.1007/s00604-022-05548-3>.
9. Corzo, D.; Tostado-Blázquez, G.; Baran, D. Flexible Electronics: Status, Challenges and Opportunities. *Front. Electron.* 2020, 1, Sec. Flexible Electronics; DOI: <https://doi.org/10.3389/felec.2020.00001>.
10. Baig, N.; Kammakakam, I.; Falath, W. Nanomaterials: A Review of Synthesis Methods, Properties, Recent Progress, and Challenges. *Mater. Adv.* 2021, 2, 1821-1871; DOI: <https://doi.org/10.1039/d0ma00807a>
11. Snyman, L.W.; Ogudo, K.D.; Foty, D. Development of a 0.75 Micron Wavelength CMOS Optical Communication System. In Proceedings of the SPIE, San Francisco, CA, USA, 2011; Volume 7943, 79430K; pp. 1–12.
12. Fang, J.; Huang, S.; Liu, F.; et al. Semi-Implantable Bioelectronics. *Nano-Micro Lett.* 14, 125 (2022). <https://doi.org/10.1007/s40820-022-00818-4>.
13. Xu, K.; Snyman, L.W.; Polleux, J.-L.; Chen, H.; Li, G. Silicon Light-Emitting Device with Application in the Micro-Opto-Electro-Mechanical Systems. *Int. J. Mater. Mech. Manuf.* 2015, 3, 282–286; ISSN 1793-8198.
14. Mariani, F.; Gualandi, I.; Schuhmann, W.; Scavetta, E. Micro- and Nano-Devices for Electrochemical Sensing. *Microchim. Acta* 189, 459 (2022). <https://doi.org/10.1007/s00604-022-05548-3>.
15. Uniyal, A.; Srivastava, G.; Pal, A.; Taya, S.; Muduli, A. Recent Advances in Optical Biosensors for Sensing Applications: a Review. *Plasmonics* 2023, 18, 735–750; DOI: <https://doi.org/10.1007/s11468-023-01803-2>.
16. O'Toole, M.; Diamond, D. Absorbance Based Light Emitting Diode Optical Sensors and Sensing Devices. *Sensors* 2008, 8, 2453–2479; DOI: <https://doi.org/10.3390/s8042453>.
17. Kishore, R.; Kumar, S.; Prasad, P. Quantum nanophotonic and nanoplasmonic sensing: towards quantum optical bioscience on a chip. *Nanophotonics* 2021, 10, 1-25; DOI: <https://doi.org/10.1515/nanoph-2020-0593>.
18. Snyman, L.W.; Polleux, J.-L.; Ogudo, K.A.; Du Plessis, M. Stimulating 600 – 650nm Wavelength Optical Emission in Monolithically Integrated Silicon LEDs through Controlled Injection-Avalanche and Carrier Density Balancing Technology. *IEEE Journal of Quantum Electronics*, 2017, 53, 1–9. doi: [10.1109/JOE.2017.2736254](https://doi.org/10.1109/JOE.2017.2736254).
19. Prostate Cancer. Available online: <https://cansa.org.za/prostate-cancer/> (accessed on 11 December 2023).
20. Bratt, O.; Auvinen, A.; Arnsrud Godtman, R.; Hellström, M.; Hugosson, J.; Lilja, H.; Wallström, J.; Roobol, M.J. Screening for Prostate Cancer: Evidence, Ongoing Trials, Policies and Knowledge Gaps. *BMJ Oncology* 2023, 2, e000039. <https://doi.org/10.1136/bmjonc-2023-000039>.
21. Hildebrandt, B. What are Normal PSA Levels by Age? Men's Hormonal Health. June 23, 2019. Online. Accessed on 13 December 2023. Available from: <https://www.menshormonalhealth.com/psa-test-results.html>.
22. Ma, K.; Zheng, Y.; An, L.; Liu, J. Ultrasensitive Immunosensor for Prostate-Specific Antigen Based on Enhanced Electrochemiluminescence by Vertically Ordered Mesoporous Silica-Nanochannel Film. *Frontiers in Chemistry*, 03 March 2022, Volume 10 - 2022. Available from: <https://doi.org/10.3389/fchem.2022.851178>.
23. Perry, G.; Cortezon-Tamarit, F.; Pascu, S.I. Detection and Monitoring Prostate Specific Antigen Using Nanotechnology. *Front. Chem. Sci. Eng.* 2020, 14(1): 4–18 <https://doi.org/10.1007/s11705-019-1846-8>.
24. Kramer, J.; Seitz, P.; Steigmeier, E.F.; Auderset, H.; Delley, B. Light-emitting devices in industrial CMOS technology. *Sensors Actuators A* 1993, 37–38, 527–533.
25. Snyman, L.W.; Aharoni, H.; du Plessis, M.; Marais, J.F.K.; Van Niekerk, D.; Biber, A. Planar Light Emitting Electro-Optical Interfaces in Standard Silicon Complementary Metal Oxide Semiconductor Integrated Circuitry. *Optical Engineering*, 2002, 41, 3230–3240.
26. Dutta, S.; Steeneken, P.G.; Agarwal, V.; Schmitz, J.; Annema, A.-J.; Hueting, R.J.E. The avalanche-mode superjunction LED. *IEEE Trans. Electron Devices* 2017, 64, 1612–1618. doi: 10.1109/TED.2017.2677340.
27. Okhai, T.A.; Snyman, L.W.; Polleux, J.-L. Wavelength Dispersion Characteristics of Integrated Silicon Avalanche LEDs – Potential Applications in Futuristic On-Chip Micro- and Nano-Bio-Sensors. *Proceedings of the SPIE Fourth Conference on Sensors, MEMS and Electro-Optic Systems (SMEOS '17)*, Skukuza, South Africa, September 2016; SPIE: 10036, 1003604. p. 1003604-1003604-22. doi: 10.1117/12.2244898.
28. Zinoviev, K.; Carascosa, L.G.; Rio, J.S.D.; Sepulveda, B.; Dominguez, C.; Lechuga, L.M. Silicon Photonic Biosensors for Lab-on-a-Chip Applications. *Adv. Opt. Technol.* 2008, 2008, 1–9. <https://doi.org/10.1155/2008/383927>.
29. Venter, P.J.; Du Plessis, M.; Bogalecki, A.W.; Goosen, M.E.; Rademeyer, P. An 8 × 64 Pixel Dot Matrix Microdisplay in 0.35 Micron CMOS Technology. *Opt. Eng.* 2012, 51, 014003.
30. Chen, A.R.; Akinwande, A.I.; Lee, H.-S. CMOS-Based Microdisplay with Calibrated Backplane. *IEEE J. Solid-State Circuits* 2005, 40, 2746–2755.
31. Rebohle, L.; Gebel, T.; Yankov, R.A.; Trautmann, T.; Skorupa, W.; Sun, J.; Gauglitz, G.; Frank, R. Microarrays of Silicon-Based Light Emitters for Novel Biosensor and Lab-on-a-Chip Applications. *Opt. Mater.* 2005, 27, 1055–1058.

32. Misiakos, K.; Petrou, P.S.; Kakabakos, S.E.; Vlahopoulou, M.E.; Tserepi, A.; Gogolides, E.; Ruf, H.H. Monolithic Silicon Optoelectronic Transducers and Elastomeric Fluidic Modules for Bio-Spotting and Bio-Assay Experiments. *Microelectron. Eng.* **2006**, *83*, 1605–1608.
33. Snyman, L.W.; Xu, K.; Polleux, J-L. Micron and Nano-Dimensioned Silicon LEDs Emitting at 650 and 750-850 nm Wavelengths in Standard Si Integrated Circuitry. *IEEE J. Quantum Electron.* **2020**, *56*, 1–8.
34. Okhai, T.A.; Idris, A.O.; Feleni, U.; et al. Nanomaterial-Enhanced Receptor Technology for Silicon On-Chip Biosensing Application. In *Biosensors - Current and Novel Strategies for Biosensing*; IntechOpen: London, UK, **2021**; doi:10.5772/intechopen.94249.
35. Hepokur, C.; Kariper, I.A.; Misir, S.; Ay, E.; Tunoglu, S.; Ersez, M.S.; Zeybek, U.; Kuruca, S.E.; Yaylim, I. Silver Nanoparticle/Capecitabine for Breast Cancer Cell Treatment. *Toxicol. In Vitro* **2019**, *61*, 104600, doi:10.1016/j.tiv.2019.104600.
36. Majeed, S.; Aripin, F.H.B.; Shoeb, N.S.B.; Danish, M.; Ibrahim, M.N.M.; Hashim, R. Bioengineered Silver Nano-Particles Capped with Bovine Serum Albumin and Its Anticancer and Apoptotic Activity against Breast, Bone and Intestinal Colon Cancer Cell Lines. *Mater. Sci. Eng. C* **2019**, *102*, 254–263.
37. Muzamil, M.; Khalid, N.; Aziz, M.D.; Abbas, S.A. Synthesis of Silver Nanoparticles by Silver Salt Reduction and Its Characterization. *Mater. Sci. Eng.* **2014**, *60*, 012034, doi:10.1088/1757-899X/60/1/012034.
38. Harisha, K.S.; Parushuram, N.; Ranjana, R.; Martis, L.J.; Narayana, B.; Sangappa, Y. Characterization and Antibacterial Properties of Biogenic Spherical Silver Nanoparticles. *Mater. Today Proc.* **2020**, *37*, 254–263.
39. Lava, M.B.; Muddapur, U.M.; Basavegowda, N.; More, S.S.; More, V.S. Characterization, Anticancer, Antibacterial, Anti-Diabetic and Anti-Inflammatory Activities of Green Synthesized Silver Nanoparticles Using *Justica Wynaadensis* Leaves Extract. *Mater. Today Proc.* **2020**, *37*, 254–263. <https://doi.org/10.1016/j.matpr.2020.10.04>.
40. Huong, V.T.L.; Thang, N.N. Green Synthesis, Characterization and Antibacterial Activity of Silver Nanoparticles Using *Sapindus Mukorossi* Fruit Pericarp Extract. *Mater. Today Proc.* **2020**, *37*, 254–263. <https://doi.org/10.1016/j.matpr.2020.10.015>.
41. Janardhanan, R.; Karuppaiah, M.; Hebalkar, N.; Rao, T.N. Synthesis and Surface Chemistry of Nano Silver Particles. *Polyhedron* **2009**, *28*, 2522–2530. <https://doi.org/10.1016/j.poly.2009.05.038>.
42. Hekmati, M.; Hasanirad, S.; Khaledi, A.; Esmaeili, D. Green Synthesis of Silver Nanoparticles Using Extracts of *Allium Rotundum* L, *Falcaria Vulgaris* Bernh, and *Ferulago Angulate* Boiss, and Their Antimicrobial Effects In Vitro. *Gene Rep.* **2020**, *19*, 1–8. <https://doi.org/10.1016/j.genrep.2020.100589>.
43. Suman, T.Y.; Radhika, S.R.; Ramkumar, R.; Rajthilak, C.; Perumal, P. The Green Synthesis of Gold Nanoparticles Using an Aqueous Root Extract of *Morinda Citrifolia* L. *Spectrochim. Acta A* **2014**, *118*, 11. <https://doi.org/10.1016/j.saa.2013.08.066>.
44. Muñoz, R.; Santos, E.M.; Galan-Vidal, C.A.; Miranda, J.M.; Lopez-Santamarina, A.; Rodriguez, J.A. Ternary quantum dots in chemical analysis. Synthesis and detection mechanisms. *Molecules* **2021**, *26*, 2764.
45. Pedano, M.L.; Rivas, G.A. Immobilization of DNA at Glassy Carbon Electrodes: A Critical Study of Adsorbed Layer. *Sensors* **2005**, *5*, 424–447. <https://doi.org/10.3390/s5060424>.
46. Popov, A.; Brasiunas, B.; Kausaite-Minkstimiene, A.; Ramanaviciene, A. Metal nanoparticle and quantum dot tags for signal amplification in electrochemical immunosensors for biomarker detection. *Chemosensors* **2021**, *9*, 85.
47. Upan, J.; Youngvises, N.; Tuantranont, A.; Karuwan, C.; Banet, P.; Aubert, P.H.; Jakmunee, J. A simple label-free electrochemical sensor for sensitive detection of alpha-fetoprotein based on specific aptamer immobilized platinum nanoparticles/carboxylated-graphene oxide. *Sci. Rep.* **2021**, *11*, 13969.
48. Hildbrandt, B. What Is a Normal PSA Level? <https://www.menshormonalhealth.com/psa-test-results.html>. (accessed Oct 7, 2023).
49. Lakkavarapu, S.; Brahman, P.K.; Reddy, K.R.; Bondili, J.S. Development of an Electrochemical Immunosensor Based on Gold Nanoparticles Incorporated Chitosan Biopolymer Nanocomposite Film for the Detection of Prostate Cancer Using PSA as Biomarker. *Enzym. Microb. Technol.* **2018**, *112*, 43–51, doi:10.1016/j.enzmictec.2017.10.009.
50. Yang, M.; Javadi, A.; Gong, S. Sensitive Electrochemical Immunosensor for the Detection of Cancer Biomarker Using Quantum Dot Functionalized Graphene Sheets as Labels. *Sens. Actuators B* **2011**, *155*, 357–360, doi:10.1016/j.snb.2010.11.055.
51. Mao, K.; Wu, D.; Li, Y.; Ma, H.; Ni, Z.; Yu, H.; Luo, C.; Wei, Q.; Du, B. Label-Free Electrochemical Immunosensor Based on Graphene/Methylene Blue Nanocomposite. *Anal. Biochem.* **2012**, *422*, 22–27, doi:10.1016/j.ab.2011.12.047.
52. Gupta, R.; Feleni, U.; Iwuoha, E. Biocompatible Osmium Telluride-Polypyrrole Nanocomposite Material: Application in Prostate Specific Antigen Immunosensing. *Processes* **2021**, *9*, 2203. <https://doi.org/10.3390/pr9122203>.
53. Khan, M.S.; Tian, L.; Liu, L.; Hu, L.; Fan, D.; Cao, W.; Wei, Q. An Ultrasensitive Electrochemical Immunosensor for the Detection of Prostate-Specific Antigen Based on Conductivity Nanocomposite with Halloysite Nanotubes. *Anal. Bioanal. Chem.* **2017**, *409*, 3245–3251, doi:10.1007/s00216-017-0266-1.

54. Martínez-Rojas, F.; Castañeda, E.; Armijo, F. Conducting Polymer Applied in a Label-Free Electrochemical Immunosensor for the Detection Prostate-Specific Antigen Using Its Redox Response as an Analytical Signal. *J. Electroanal. Chem.* 2021, 880, 114877, doi:10.1016/j.jelechem.2020.114877.
55. Kavosi, B.; Salimi, A.; Hallaj, R.; Moradi, F. Ultrasensitive Electrochemical Immunosensor for PSA Biomarker Detection in Prostate Cancer Cells Using Gold Nanoparticles/PAMAM Dendrimer Loaded with Enzyme Linked Aptamer as Integrated Triple Signal Amplification Strategy. *Biosens. Bioelectron.* 2015, 74, 915–923, doi:10.1016/j.bios.2015.07.064.
56. Suresh, L.; Bondili, J.S.; Brahman, P.K. Development of Proof of Concept for Prostate Cancer Detection: An Electrochemical Immunosensor Based on Fullerene-C60 and Copper Nanoparticles Composite Film as Diagnostic Tool. *Mater. Today Chem.* 2020, 16, 100257, doi:10.1016/j.mtchem.2020.100257.
57. Oliveira, N.; Costa-Rama, E.; Viswanathan, S.; Delerue-Matos, C.; Pereira, L.; Morais, S. Label-free Voltammetric Immunosensor for Prostate Specific Antigen Detection. *Electroanalysis* 2018, 30, 2604–2611.
58. Jang, H.D.; Kim, S.K.; Chang, H.; Choi, J.-W. 3D Label-Free Prostate Specific Antigen (PSA) Immunosensor Based on Graphene–Gold Composites. *Biosens. Bioelectron.* 2015, 63, 546–551, doi:10.1016/j.bios.2014.08.008.
59. Ji, S.; Lee, M.; Kim, D. Detection of Early Stage Prostate Cancer by Using a Simple Carbon Nanotube@Paper Biosensor. *Biosens. Bioelectron.* 2018, 102, 345–350, doi:10.1016/j.bios.2017.11.035.
60. Johnson, E.D.; Kotowski, T.M. Detection of Prostate Specific Antigen by ELISA. *J. Forensic Sci.* 1993, 38(2), 250–258. <https://doi.org/10.1520/JFS13403J>.

**Disclaimer/Publisher's Note:** The statements, opinions and data contained in all publications are solely those of the individual author(s) and contributor(s) and not of MDPI and/or the editor(s). MDPI and/or the editor(s) disclaim responsibility for any injury to people or property resulting from any ideas, methods, instructions or products referred to in the content.